Active Frequency Measurement on Superradiant Strontium Clock Transitions

Yuan Zhang,[1,*] Chongxin Shan,[1,†] and Klaus Mølmer[2,‡]

[1]Henan Key Laboratory of Diamond Optoelectronic Materials and Devices, Key Laboratory of Material Physics Ministry of Education, School of Physics and Microelectronics, Zhengzhou University, Daxue Road 75, Zhengzhou 450052, China

[2]Center for Complex Quantum Systems, Department of Physics and Astronomy, Aarhus University, Ny Munkegade 120, DK-8000 Aarhus C, Denmark and Aarhus Institute of Advanced Studies, Aarhus University, Høegh-Guldbergs Gade 6B, DK-8000 Aarhus C, Denmark

(Received 25 June 2021; accepted 13 December 2021; published 7 January 2022)

We develop a stochastic mean-field theory to describe active frequency measurements of pulsed superradiant emission, studied in a recent experiment with strontium-87 atoms trapped in an optical lattice inside an optical cavity [M. Norcia *et al.*, Phys. Rev. X **8**, 021036 (2018)]. Our theory reveals the intriguing dynamics of atomic ensembles with multiple transition frequencies, and it reproduces the superradiant beats signal, noisy power spectra, and frequency uncertainty in remarkable agreement with the experiments. Moreover, using longer superradiant pulses of similar strength and shortening the experimental duty cycle, we predict a short-term frequency uncertainty $7 \times 10^{-17}/\sqrt{\tau/s}$, which makes active frequency measurements with superradiant transitions comparable with the record performance of current frequency standards [M. Schioppo *et al.*, Nat. Photonics **11**, 48 (2017)]. Our theory combines cavity quantum electrodynamics and quantum measurement theory, and it can be readily applied to explore conditional quantum dynamics and describe frequency measurements for other processes such as steady-state superradiance and superradiant Raman lasing.

DOI: 10.1103/PhysRevLett.128.013604

Introduction.—Optical clocks possess superior precision and accuracy compared to their counterparts in the microwave domain [1]. The pursuit of optical clocks follows two paths with either single trapped ions, which allow long interrogation time and achieve impressive frequency resolution [2], or ensembles of neutral alkaline-earth atoms, which can provide a better signal-to-noise ratio and can be also trapped in optical lattices to reduce the Doppler broadening [3]. Beyond quantum metrology [4], trapped ions and alkaline-earth atoms are also useful for the exploration of quantum computing [5] and simulation, as well as many-body spin physics [6,7].

Most optical clocks are based on a passive scheme [1], where a driving field excites atoms and its frequency is matched to the atomic transition frequency by monitoring the atomic population dynamics via fluorescence detection. Alternatively, in an active scheme, the atomic transition frequency is measured by comparing the emitted signal with a reference laser. While the passive scheme has superior long-term stability and absolute accuracy, the active scheme offers a wide detection bandwidth and dynamical range. The active scheme has been implemented in the microwave domain with hydrogen masers [8]. Recently, M. Norcia *et al.* [9] demonstrated active frequency measurements of pulsed superradiance of strontium atoms on the optical clock transition in the optical domain.

The system studied in [9] consists of more than 10^5 strontium-87 atoms trapped in a one-dimensional optical lattice inside an optical cavity; see Fig. 1(a). The ^{87}Sr atoms have nuclear spin $F = 9/2$, and subject to a magnetic field, the hyper-fine levels of the electronic ground $^1S_0$ and excited state $^3P_0$ are Zeeman split and give rise to a number of $\sigma^{\pm}$ and π transitions; see Fig. 1(b). The atoms couple to a cavity mode with vertical polarization via the π transitions, which can be labeled with the quantum number $m_F = -F, -F+1, \ldots, F$.

The procedure adopted in [9] [Fig. 1(a)] can be summarized as follows: (i) the atoms are initially prepared in a mixture of different sublevels of the ground state with

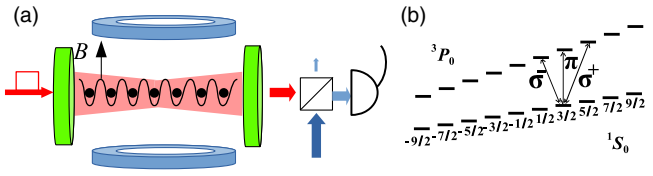

FIG. 1. Panel (a) shows an ensemble of lattice trapped ^{87}Sr atoms in a cavity, which are subject to a magnetic field and heterodyne detection by photon counting on the beam mixing the superradiance from the cavity (horizontal fat red arrow) and a reference laser (vertical long blue arrow). Panel (b) shows hyperfine levels labeled by $m_F = -F, -F+1, \ldots F$ ($F = 9/2$) of the electronic ground $^1S_0$ and excited $^3P_0$ states and three kinds of transitions: σ^+, π, σ^- (with $\Delta m_F = +1, 0, -1$). By defining the quantization axis with a vertical magnetic field, the cavity mode with vertical polarization couples only to the atomic π transitions.

proper laser pulse sequences; (ii) a laser pulse drives the cavity to excite the atoms; (iii) the excited atoms interact collectively with the cavity mode resulting in pulsed superradiance; (iv) the superradiance signal interferes with a reference laser and is measured with a photo detector; (v) the Fourier transform of the photo current leads to the power spectral intensity, from which the atomic transition frequencies are inferred. Following this procedure, a frequency uncertainty of 6.7×10^{-16} is achieved after one second of integration time [9]. We note that in [10], the initial atomic excitation is realized by chirped adiabatic passage. Since the superradiance is much faster than the individual atom decay via $\sigma^{\pm}$ and π transitions, the number of atoms contributing to each superradiant π transition does not change during the experiment and the whole atom ensemble can be viewed as ten separate subensembles with different transition frequencies.

In this Letter, we apply a mean-field approach based on cumulant expansions to describe cavity quantum electrodynamics (QED) theory with many emitters [11,12], and we develop this theory further to incorporate the stochastic measurement back action due to the continuous probing of the system, which has so far been restricted to small systems, via stochastic master equations [13]. While applied here to high precision frequency measurement, our theory reveals how to generally incorporate measurement back action in systematic mean-field theories and holds potential for exploration of a range of quantum measurement effects in many-body systems and large systems, intractable by usual master equation approaches. Our simulations show that the frequency uncertainty can be reduced by 1 to 2 orders of magnitude by using longer superradiance pulses of similar strength and by reducing the time for single measurements. The optimized uncertainty becomes comparable with the current record 6×10^{-17} at one second [14].

Stochastic master equation for conditional dynamics.—In the following, we present the stochastic master equation for the conditioned density operator $\hat{\rho}$:

$$\frac{\partial}{\partial t}\hat{\rho} = \left(\frac{\partial}{\partial t}\hat{\rho}\right)_p + \left(\frac{\partial}{\partial t}\hat{\rho}\right)_s + \left(\frac{\partial}{\partial t}\hat{\rho}\right)_d. \tag{1}$$

The first term,

$$\left(\frac{\partial}{\partial t}\hat{\rho}\right)_p = -\frac{i}{\hbar}[\hat{H}_c + \hat{H}_d, \hat{\rho}] - \frac{\kappa}{2}(\{\hat{a}^+\hat{a}, \hat{\rho}\} - 2\hat{a}\hat{\rho}\hat{a}^+), \tag{2}$$

specifies the cavity mode Hamiltonian $\hat{H}_c = \hbar\omega_c \hat{a}^+\hat{a}$ with frequency ω_c, photon creation $\hat{a}^+$ and annihilation operator $\hat{a}$, and the driving of the cavity mode $\hat{H}_d = \sqrt{\kappa_1}\hbar\beta(t)e^{i\omega_d t}\hat{a} + \text{H.c.}$ by a laser pulse with a frequency ω_d and a time-dependent strength $\beta(t)$ through the left mirror. The remaining term describes the photon loss with a rate $\kappa = \kappa_1 + \kappa_2$ due to the left ($\kappa_1 = 2\pi \times 72.5$ kHz) and right ($\kappa_2 = \kappa_1$) mirror.

The second part of Eq. (1),

$$\left(\frac{\partial}{\partial t}\hat{\rho}\right)_s = -\frac{i}{\hbar}[\hat{H}_a + \hat{H}_{a-c}, \hat{\rho}], \tag{3}$$

specifies the Hamiltonian $\hat{H}_a = \hbar \sum_{i=1}^{10} (\omega_i/2) \sum_{k=1}^{N_i} \hat{\sigma}^z_{i,k}$ of ten subensembles (indicated by "$i = m_F$") of N_i atoms (labeled with "k"), associated with the ten π transitions of frequencies $\omega_{i=m_F} = \omega_a + \Delta_B m_F$ and Pauli operator $\hat{\sigma}^z_{i,k}$. $\omega_{i=m_F}$ are given by the intrinsic atomic transition frequency $\omega_a/2\pi = 429.5$ THz (corresponding to a wavelength of 698 nm) and the constant $\Delta_B = 2\pi \times 108.4 \times B$ Hz for the static magnetic field B in Gauss [9]. The Hamiltonian $\hat{H}_{a-c} = \hbar \sum_i g_i[\hat{a}^+(\sum_k \hat{\sigma}^-_{i,k}) + (\sum_k \hat{\sigma}^+_{i,k})\hat{a}]$ describes the atom-cavity mode coupling with the lowering $\hat{\sigma}^-_{i,k}$ and raising $\hat{\sigma}^+_{i,k}$ operators and the strengths $g_{i=m_F} = g_0 m_F/\sqrt{F(F+1)}$ (with $g_0 = 2\pi \times 2.41$ Hz). Here, we assume that all the atoms in the ith subensemble have the same ω_i and g_i, and we have ignored the negligible spontaneous emission rate and dephasing rate in the optical lattice clock system.

The third part of Eq. (1) describes the measurement back action due to the heterodyne detection:

$$\left(\frac{\partial}{\partial t}\hat{\rho}\right)_d = \frac{dW}{dt}\sqrt{\eta\kappa_2}[e^{i\omega_l t}(\hat{a} - \langle\hat{a}\rangle)\hat{\rho} + \hat{\rho}e^{-i\omega_l t}(\hat{a}^+ - \langle\hat{a}\rangle^*)]. \tag{4}$$

Here, the random number dW describes the detector photon-shot noise and follows a normal distribution with a variance $dW(t)^2 = dt$ and a mean $E[dW(t)] = 0$. The parameter η accounts for the photo-counting efficiency of the detector. In the heterodyne detection, the signal beam from the cavity is mixed with a local oscillator of frequency ω_l on a single photodetector [Fig. 1(a)], and a large constant signal component due to the local oscillator intensity is subtracted to reveal the interference term, linear in cavity field amplitude $\langle\hat{a}\rangle$,

$$J(t) = \sqrt{\eta\kappa_2}2\text{Re}[e^{i\omega_l t}\langle\hat{a}\rangle] + dW/dt, \tag{5}$$

which is dominated by the detector photon-shot noise dW/dt. The derivation of Eqs. (4) and (5) is presented, e.g., in Sec. 4.4 and Sec. 4.5 of [13].

To simulate tens of thousands of atoms in the experiments and to account properly for the collective atom-cavity mode interaction, we solve Eq. (1) with second-order mean-field theory [12,15], equivalent to the cluster expansion approach [16], by deriving the equation $\partial_t\langle\hat{o}\rangle = \text{tr}\{\hat{o}\partial_t\hat{\rho}\}$ for the expectation value $\langle\hat{o}\rangle$ of any observable $\hat{o}$. Following this procedure, we obtain the equation for the intra-cavity photon number:

$$\frac{\partial}{\partial t}\langle\hat{a}^+\hat{a}\rangle = -2\sqrt{\kappa_1}\mathrm{Im}[\beta(t)e^{i\omega_d t}\langle\hat{a}\rangle] - \kappa\langle\hat{a}^+\hat{a}\rangle - 2\sum_i g_i N_i \mathrm{Im}\langle\hat{a}\hat{\sigma}_i^+\rangle + \frac{dW}{dt}\sqrt{\eta\kappa_2}2\mathrm{Re}[e^{-i\omega_l t}(\langle\hat{a}^+\hat{a}^+\hat{a}\rangle - \langle\hat{a}\rangle^*\langle\hat{a}^+\hat{a}\rangle)], \tag{6}$$

which depends on the cavity field amplitude $\langle\hat{a}\rangle$, the atom-photon correlation $\langle\hat{a}\hat{\sigma}_i^+\rangle$, and higher order correlations $\langle\hat{a}^+\hat{a}^+\hat{a}\rangle$. To close the equations, we approximate the third-order correlations $\langle\hat{o}\,\hat{p}\,\hat{q}\rangle$ with lower-order correlations $\langle\hat{o}\rangle\langle\hat{p}\,\hat{q}\rangle + \langle\hat{p}\rangle\langle\hat{o}\,\hat{q}\rangle + \langle\hat{q}\rangle\langle\hat{o}\,\hat{p}\rangle - 2\langle\hat{o}\rangle\langle\hat{p}\rangle\langle\hat{q}\rangle$ (for any operators $\hat{o}, \hat{p}, \hat{q}$) [11]. The cavity field amplitude then obeys the equation

$$\frac{\partial}{\partial t}\langle\hat{a}\rangle = -i(\omega_c - i\kappa/2)\langle\hat{a}\rangle - i\sqrt{\kappa_1}\beta^*(t)e^{-i\omega_d t} - i\sum_i g_i N_i\langle\hat{\sigma}_i^-\rangle + \frac{dW}{dt}\sqrt{\eta\kappa_2}[e^{-i\omega_l t}(\langle\hat{a}^+\hat{a}\rangle - |\langle\hat{a}\rangle|^2) + e^{i\omega_l t}(\langle\hat{a}^2\rangle - \langle\hat{a}\rangle^2)]. \tag{7}$$

The equations for $\langle\hat{a}\hat{\sigma}_i^+\rangle$ and other terms, e.g., the atomic population difference $\langle\hat{\sigma}_i^z\rangle$ and coherence $\langle\hat{\sigma}_i^-\rangle$, are detailed in Sec. S1 of [17]. In the above equations and those in Sec. S1, we assume all the atoms identical so that the sum of the identical quantities like $\langle\hat{a}\hat{\sigma}_{i,k}^+\rangle, \langle\hat{\sigma}_{i,k}^-\hat{\sigma}_{i,k'}^+\rangle, \langle\hat{\sigma}_{i,k}^-\hat{\sigma}_{j,k'}^+\rangle$ (with $k \neq k'$) for any atom k and any atomic pair (k, k') can be replaced by the product of representative quantities, e.g., $\langle\hat{a}\hat{\sigma}_i^+\rangle, \langle\hat{\sigma}_i^-\hat{\sigma}_i^+\rangle, \langle\hat{\sigma}_i^-\hat{\sigma}_j^+\rangle$ with factors, e.g., $N_i, N_i - 1, N_j$. In this way, we reduce dramatically the number of independent quantities.

Frequency measurement using superradiance pulses.—We apply the above stochastic mean-field equations to simulate the frequency measurements on the pulsed superradiance, as reported in [9]. To obtain Fig. 2, we assume $\omega_c = \omega_a$ and a magnetic field of about 1.537 Gauss, resulting in ten π transitions with frequencies $\omega_{\pm 9/2,\pm 7/2,\pm 5/2,\pm 3/2,\pm 1/2}/2\pi = \omega_a/2\pi \pm 750.00$, 583.33, 416.67, 250.00, 83.33 Hz. We drive the cavity resonantly ($\omega_d = \omega_c$) by a square laser pulse of a duration $T = 11.5$ ms and a coupling strength $\beta(t) = 2\pi \times 7.5 \times 10^3\sqrt{\mathrm{Hz}}$, and we then switch on the heterodyne detection with a local oscillator of frequency $\omega_l = \omega_c + 2\pi$ kHz and a detection efficiency $\eta = 0.12$ [9].

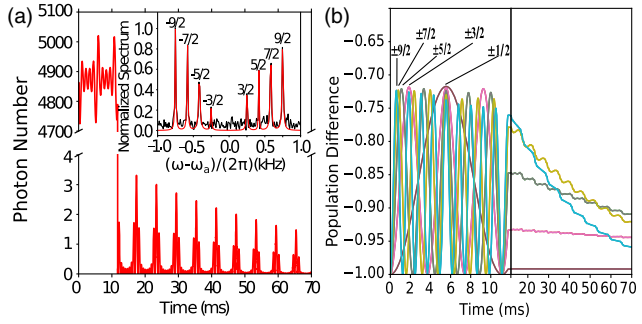

FIG. 2. Preparation, superradiance, and heterodyne detection of 4×10^5 ^{87}Sr atoms evenly distributed over ten transitions with $m_F = \pm 9/2, \ldots, \pm 1/2$. Panels (a) and (b) show the intra-cavity photon number and population difference among the excited and ground states for each m_F. The inset in panel (a) shows the simulated power spectral density (black noisy curve) and Lorentzian fits to the spectral peaks (red solid curves). The simulation parameters are specified in the text.

Figure 2(a) shows that the intra-cavity photon number increases dramatically and oscillates around 4850 when the driving laser is on, drops dramatically when it is off, and finally yields a complex beat pattern, in good agreement with Fig. 2(c) in [9]. Figure 2(b) shows that the population difference $\langle\hat{\sigma}_{m_F}^z\rangle$ of different subensembles follows oscillations of different periods in the preparation stage (0 to 11.5 ms) and then decays monotonically with small ripples in the superradiant stage (11.5 to 70 ms).

These results can be understood by noting that for a laser pulse with amplitude $\sqrt{\kappa_1}\beta \gg \kappa$, the field inside the cavity behaves like a classical field with an amplitude $\langle\hat{a}\rangle \approx i2\sqrt{\kappa_1}\beta/\kappa$ (for $\omega_c = \omega_d$). Such a classical field would drive the atoms to follow the Rabi oscillations, and the population difference is given by $\langle\hat{\sigma}_{m_F}^z\rangle = 2P_e^{\max}\sin^2(|m_F|\Omega_0 T/2) - 1$ with $P_e^{\max} = |2\langle\hat{a}\rangle g_0/\Omega_0\sqrt{F(F+1)}|^2$ and $\Omega_0 = \sqrt{\Delta_B^2 + |2\langle\hat{a}\rangle g_0/\sqrt{F(F+1)}|^2}$, which are both independent of m_F; see Sec. S2 B of [17]. The Rabi frequencies $|m_F|\Omega_0$ lead to faster oscillation of $\langle\hat{\sigma}_{m_F}^z\rangle$ for larger $|m_F|$ and same population at integer multiples of the period $2\pi/\Omega_0$. For the current system, we estimate $|\langle a\rangle| \approx 70$ and $\Omega_0 \approx 2\pi \times 180$ Hz and calculate $P_e^{\max} \approx 0.142$ and then $2P_e^{\max} - 1 \approx -0.72$, close to the maximal $\langle\hat{\sigma}_{m_F}^z\rangle$ shown in Fig. 2(b). Here, the low atomic excitation is mostly because the atomic subensembles are off-resonant with the cavity field. To reproduce the superradiant pattern in the experiment [9], we choose T such that $\langle\hat{\sigma}_{m_F}^z\rangle$ decreases with reducing $|m_F|$; see the curve crossings with the vertical line in Fig. 2(b). In the superradiant stage, $\langle\hat{\sigma}_{m_F}^z\rangle$ decays faster for the subensembles with larger $|m_F|$, reflecting the larger Purcell enhanced atomic decay rate $\Gamma_{m_F} = [m_F g_0/\sqrt{F(F+1)}]^2(\kappa/2)/[m_F^2\Delta_B^2 + \kappa^2/4]$ for larger $|m_F|$ (notice $|m_F|\Delta_B \ll \kappa/2$). In addition, it also shows small steps caused by the constructive and destructive interference between the atomic subensembles (not shown).

The heterodyne detection yields a fluctuating photon current (see Sec. S2 A of [17]), and the Fourier transform of this signal yields a power spectral density with eight peaks, which are fitted by Lorentzian functions with the frequencies $(\omega_{m_F} - \omega_a)/2\pi = -750.60, -582.53, -416.41, -251.76$ Hz for $m_F = -9/2, \ldots, -3/2$ and $(\omega_{m_F} - \omega_a)/2\pi = 250.61, 415.69, 582.91, 749.53$ Hz for $m_F = 3/2, \ldots, 9/2$;

see the inset of Fig. 2(a). The transitions $m_F = \pm 1/2$ with frequencies $\omega_{\pm 1/2}$ couple too weakly with the cavity mode to be resolved. The difference between the extracted and expected frequencies is caused by the detection noise and contributes to the frequency uncertainty (see below).

Uncertainty of the frequency measurement.—So far, we consider atoms distributed over all the π transitions. It may be better to distribute the atoms only to the two extreme transitions $m_F = \pm 9/2$ since they couple more strongly with the cavity mode and provide also two symmetrically separated peaks in the power spectral density, which are sufficient to determine the intrinsic atomic transition frequency. Figure 3 demonstrates the frequency measurement for such a system with 1.8×10^5 ^{87}Sr atoms, a magnetic field of 0.943 Gauss, resulting in the transition frequencies $\omega_{\pm 9/2}/2\pi = \omega_a/2\pi \pm 460$ Hz, and a laser pulse of a strength $\beta(t) = 2\pi \times 5 \times 10^3\ \sqrt{\text{Hz}}$ and a duration 8.8 ms. Figure 3(a) shows similar results as Fig. 2(a) except for simpler beats signal and two peaks in the power spectral density, which are consistent with Fig. 2(b) in [9]. The extracted frequencies of the two peaks are $(\omega_{-9/2,9/2} - \omega_a)/2\pi = -460.31$, 459.91 Hz and deviate from the expected values by 0.31 Hz and 0.09 Hz.

The uncertainty of the frequency measurement as a function of the total duration τ of the experiment is characterized by the so-called fractional Allan deviation $\sigma(\tau)$ [1]. To compute this quantity, let us assume that we need the time T_c to carry out a single experiment, e.g., $T_c = 1.1$ s in [9], and that we have carried out N experiments to yield N candidate frequencies $\bar{\omega}_n$. Then, $\sigma(\tau)$ for the probing time $\tau = T_c$ can be evaluated with $\sigma(\tau) = \sqrt{[1/(N-1)]\sum_{n=1}^{N-1}(\bar{\omega}_{n+1} - \bar{\omega}_n)^2/(2\omega_a^2)}$. Consistent with the experiment [9], we consider the average of m frequencies ($m < N/2$) as the frequency measured with a single experiment of total duration $\tau = mT_c$, and we thus obtain N/m average frequencies by which we compute $\sigma(\tau)$ for $\tau = mT_c$. This treatment leads to a precise estimate of $\sigma(\tau)$ for short τ, while the smaller sample size available for longer τ makes the estimate of $\sigma(\tau)$ correspondingly less precise. This feature of $\sigma(\tau)$ is also visible in Fig. 3(a) of [9].

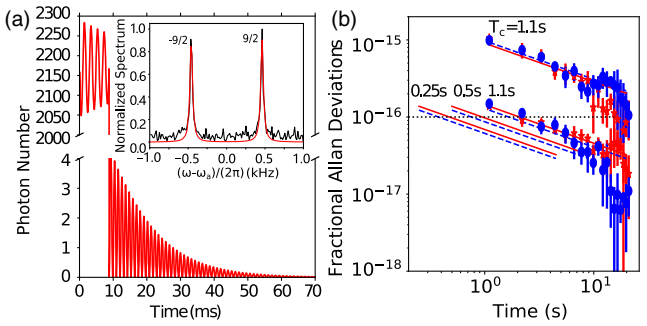

FIG. 3. Frequency measurement on pulsed superradiance from 1.8×10^5 ^{87}Sr atoms distributed evenly on the two extreme $m_F = \pm 9/2$ atomic transitions. Panel (a) shows similar results as Fig. 2(a). Panel (b) shows the fractional Allan deviation $\sigma(\tau)$ for the center (red asterisks) and difference (blue dots) of the peak frequencies $\omega_{\pm 9/2}$. The mean and standard deviation are obtained by averaging the frequencies over 3×40 independent simulations, each lasting for $T_c = 1.1$ s [9]. The upper asterisks and dots are for the system considered in panel (a), while the lower ones are for optimized system parameters giving longer superradiance pulses of similar strength. The results of the fitting of these data (red solid and blue dashed lines) are explained in the text. The leftmost pairs of red solid and blue dashed lines show the results for $T_c = 0.5$ and 0.25 s. The horizontal dotted line shows the noise floor 10^{-16} of the reference laser used in [9]. Other parameters are specified in the text.

Figure 3(b) shows the computed $\sigma(\tau)$ for the center frequency $\omega_{\text{cen}} = (\omega_{9/2} + \omega_{-9/2})/2$ (red asterisks) and the frequency difference $\omega_{\text{dif}} = (\omega_{9/2} - \omega_{-9/2})/2$ (blue dots). For ω_{cen}, $\sigma(\tau)$ can be fitted with $9.06 \times 10^{-16}/\sqrt{\tau/s}$ in good agreement with the measured value $\sigma(\tau) = 1.04 \times 10^{-15}/\sqrt{\tau/s}$ [9]. However, for ω_{dif}, $\sigma(\tau)$ can be fitted with $9.75 \times 10^{-16}/\sqrt{\tau/s}$, which is about 2 times larger than the measured value $\sigma(\tau) = 4.5 \times 10^{-16}/\sqrt{\tau/s}$ in [9]. The photon-shot noise should in principle lead to the same uncertainty for ω_{cen} and ω_{dif}, while the larger uncertainty for ω_{cen} than ω_{dif} in the experiment may be caused by other processes affecting the two superradiant peaks in the same manner, such as noise of the reference laser, cavity pulling effects, and shifts associated with the atomic density, as pointed out in [9]. In view of the possible variations of many parameters in separate experiments, such as the atomic numbers, the driving field, and the reference laser, the agreement of the measured and calculated $\sigma(\tau)$ is quite remarkable. In particular, we note that it was mentioned in [9] that superradiant pulses with lengths $\lesssim 100$ ms were used for $\sigma(\tau)$ estimation, while the pulses are only 40 ms long in our simulations. Based on this observation, we may assume that our simulations yield the same or upper bound of the Allan deviation of the frequency measurements.

To optimize the frequency measurement, we notice that the duration of the superradiant pulse is inversely proportional to the number of atoms N [10] and can be affected by the atomic initial states and the magnetic field; see Sec. S2 B in [17]. Thus, by reducing N to 9×10^4 and assuming a smaller Zeeman splitting for the transition frequencies, $\omega_{\pm 9/2} = \omega_a \pm 2\pi \times 50$ Hz, and using a rectangle laser pulse of strength $\beta(t) = 2\pi \times 10^4\sqrt{\text{Hz}}$ and shorter duration $T = 1.1$ ms, we can prepare the atoms with more than 97% population in the excited state and obtain a 300 ms long superradiant-beat signal of similar strength, leading to two frequency peaks; see Sec. S2 C of [17]. These peaks lead to $\sigma(\tau) = 1.44, 1.29 \times 10^{-16}/\sqrt{\tau/s}$ for ω_{cen} and ω_{dif}, respectively; see the rightmost red solid and blue dashed lines in Fig. 3(b).

Before we can achieve the predicted $\sigma(\tau)$, we must address two obstacles. In the experiment [9], the reference

laser is stabilized with a high-quality optical cavity, which has a thermal noise floor of 1×10^{-16} [see the horizontal dashed line in Fig. 3(b)], and the atoms are lost during single measurement and new atoms must be reloaded into the cavity for a new experiment, which leads to the total time $T_c = 1.1$ s or longer for a single experiment. To overcome these obstacles, we can reduce the noise level of the reference laser by stabilizing it to an ultra high–quality optical cavity, and we may compensate the atom loss by continuously injecting new atoms [20]; see Sec. S2 D in [17]. If we can reduce the time for single experiments to, e.g., $T_c = 0.5$ s or 0.25 s, $\sigma(\tau)$ can be reduced to $9 \times 10^{-17}/\sqrt{\tau/s}$ or $7 \times 10^{-17}/\sqrt{\tau/s}$, as indicated with the leftmost pairs of blue dashed and red solid lines in Fig. 3(b), which become comparable with the record $6 \times 10^{-17}/\sqrt{\tau/s}$ [14].

In the above simulations, the atoms are initially prepared in superposition states, leading to an initial atomic coherence, $\langle \hat{\sigma}_i^- \rangle \neq 0$. According to Eq. (7), this coherence feeds the cavity field amplitude $\langle \hat{a} \rangle \neq 0$ and drives the photon current in the heterodyne detection [see Eq. (5)], allowing us to detect the frequencies. In these simulations, the randomness associated with the measurement yields the noise in the detected signal, which determines the short-term uncertainty of frequency measurement, while the measurement back action does not affect the system dynamics appreciably. However, for atoms prepared in the fully excited state, there is no initial atomic coherence and hence no mean optical coherence, but in every single shot of the experiment, the measurement back action causes a breaking of the symmetry to establish optical coherence in the system and thus yields a modulated heterodyne current; see Sec. S2 E of [17].

Conclusion.—In summary, we have combined the theory of continuous quantum measurements and a mean-field description of cavity QED with many emitters to simulate heterodyne detection of pulsed superradiance from tens of thousands of ^{87}Sr atoms trapped in a one-dimensional optical lattice inside an optical cavity. Our simulations show that the computed frequency uncertainty decreases as $\sim 9 \times 10^{-16}/\sqrt{\tau/s}$ with the measurement time τ, in agreement with the recent experiment [9]. By use of longer superradiance pulses of similar strength and a shorter duty cycle for single measurements, the frequency uncertainty may be further reduced by 1 to 2 orders of magnitude and thus become comparable with current records [14].

Our theory can be directly applied to the study of frequency measurements on superradiant pulses from other alkaline-earth atoms such as strontium-88 atoms [21,22] and calcium atoms [23]. Steady-state superradiance [11] and superradiant Raman lasers [24] may be subject to similar analyses, which may also reveal more exotic effects of quantum measurements such as conditional entanglement and spin squeezing.

The authors thank James K. Thompson for generously sharing details and insights from the experiments on superradiance frequency measurements [9,10]. This work was supported by the National Natural Science Foundation of China through the Project No. 12004344 and the Danish National Research Foundation through the Grant Agreement No. DNRF156.

*Corresponding author.
yzhuaudipc@zzu.edu.cn
†Corresponding author.
cxshan@zzu.edu.cn
‡Corresponding author.
moelmer@phys.au.dk

[1] A. D. Ludlow, M. M. Boyd, J. Ye, E. Peik, and P. O. Schmidt, Optical atomic clocks, Rev. Mod. Phys. **87**, 637 (2015).
[2] W. H. Oskay, S. A. Diddams, E. A. Donley, T. M. Fortier, T. P. Heavner, L. Hollberg, W. M. Itano, S. R. Jefferts, M. J. Delaney, K. Kim, F. Levi, T. E. Parker, and J. C. Bergquist, Single-Atom Optical Clock with High Accuracy, Phys. Rev. Lett. **97**, 020801 (2006).
[3] M. M. Boyd, High precision spectroscopy of strontium in an optical lattice: Towards a new standard for frequency and time, Ph.D. thesis, University of Washington, 2002.
[4] J. Ye, H. J. Kimble, and H. Katori, Quantum state engineering and precision metrology using state-insensitive light traps, Science **320**, 1734 (2008).
[5] J. J. García-Ripoll, P. Zoller, and J. I. Cirac, Quantum information processing with cold atoms and trapped ions, J. Phys. B **38**, S567 (2005).
[6] M. J. Martin, M. Bishof, M. D. Swallows, X. Zhang, C. Benko, J. Von-Stecher, A. V. Gorshkov, A. M. Rey, and J. Ye, A quantum many-body spin system in an optical lattice clock, Science **341**, 632 (2013).
[7] K. Kim, M.-S. Chang, S. Korenblit, R. Islam, E. E. Edwards, J. K. Freericks, G.-D. Lin, L.-M. Duan, and C. Monroe, Quantum simulation of frustrated ising spins with trapped ions, Nature (London) **465**, 590 (2010).
[8] M. A. Weiss and F. L Walls, Preliminary evaluation of time scales based on hydrogen masers, IEEE Trans. Instrum. Meas. **45**, 265 (1996).
[9] M. A. Norcia, J. R. K. Cline, J. A. Muniz, J. M. Robinson, R. B. Hutson, A. Goban, G. E. Marti, J. Ye, and J. K. Thompson, Frequency Measurements of Superradiance from the Strontium Clock Transition, Phys. Rev. X **8**, 021036 (2018).
[10] M. A. Norcia, M. N. Winchester, J. R. K. Cline, and J. K. Thompson, Superradiance on the millihertz linewidth strontium clock transition, Sci. Adv. **2**, e1601231 (2016).
[11] D. Meiser, J. Ye, D. R. Carlson, and M. J. Holland, Prospects for a Millihertz-Linewidth Laser, Phys. Rev. Lett. **102**, 163601 (2009).
[12] K. Debnath, Y. Zhang, and K. Mølmer, Lasing in the superradiant crossover regime, Phys. Rev. A **98**, 063837 (2018).

[13] H. M. Wiseman and G. J. Milburn, *Quantum Measurement and Control* (Cambridge University Press, Cambridge, England, 2009), pp. 157–166.
[14] M. Schioppo, R. C. Brown, W. F. McGrew, N. Hinkley, R. J. Fasano, K. Beloy, T. H. Yoon, G. Milani, D. Nicolodi, J. A. Sherman, N. B. Phillips, C. W. Oates, and A. D. Ludlow, Ultra-stable optical clock with two cold-atom ensembles, Nat. Photonics **11**, 48 (2017).
[15] Y. Zhang, C. X. Shan, and K. Mølmer, Ultra-Narrow Superradiant Lasing by Dark Atom-Photon Dressed States, Phys. Rev. Lett. **126**, 123602 (2021).
[16] H. A. M. Leymann, A. Foerster, and J. Wiersig, Expectation value based equation-of-motion approach for open quantum systems: A general formalism, Phys. Rev. B **89**, 085308 (2014).
[17] See Supplemental Material, which includes Refs. [18,19], at http://link.aps.org/supplemental/10.1103/PhysRevLett.128.013604 for additional details.
[18] Y. Zhang, Y. X. Zhang, and K. Mølmer, Monte-Carlo simulations of superradiant lasing, New J. Phys. **20**, 112001 (2018).
[19] Q. Xu, E. Greplova, B. Julsgaard, and K. Mølmer, Correlation functions and conditioned quantum dynamics in photodetection theory, Phys. Scr. **90**, 128004 (2015).
[20] C.-C. Chen, S. Bennetts, R. G. Escudero, B. Pasquiou, and F. Schreck, Continuous Guided Strontium Beam with High Phase-Space Density, Phys. Rev. Applied **12**, 044014 (2019).
[21] S. A. Schäffer, M. Tang, M. R. Henriksen, A. A. Jørgensen, B. T. R. Christensen, and J. W. Thomsen, Lasing on a narrow transition in a cold thermal strontium ensemble, Phys. Rev. A **101**, 013819 (2020).
[22] M. A. Norcia and J. K. Thompson, Cold-strontium Laser in the Superradiant Crossover Regime, Phys. Rev. X **6**, 011025 (2016).
[23] T. Laske, H. Winter, and A. Hemmerich, Pulse Delay Time Statistics in a Superradiant Laser with Calcium Atoms, Phys. Rev. Lett. **123**, 103601 (2019).
[24] J. M. Weiner, K. C. Cox, J. G. Bohnet, Z. Chen, and J. K. Thompson, Superradiant Raman laser magnetometer, Appl. Phys. Lett. **101**, 261107 (2012).